crystals

MDPI

Article

Structure Tuning of Hafnium Metal–Organic Frameworks through a Mixed Solvent Approach

Yanhong Ma [1] and Xin Zhang [2,*]

[1] Department of Intelligent Optoelectronic Technology Application, School of Microelectronics, Shenzhen Institute of Information Technology, Shenzhen 518172, China; mayh1986@icloud.com
[2] Beijing Key Laboratory for Green Catalysis and Separation, Department of Environmental Chemical Engineering, Faculty of Environment and Life, Beijing University of Technology, Beijing 100124, China
* Correspondence: zhang.xin@bjut.edu.cn

Abstract: The recent development of water-stable metal–organic frameworks (MOFs) has significantly broadened the application scope of this emerging type of porous material. Structure tuning of hafnium MOFs is less studied compared with zirconium MOFs. In this work, we report the synthesis of a mesoporous hafnium MOF, csq-MOF-1, through finely tuning the solvent mixture ratio. The successful synthesis of csq-MOF-1 also relies on the linker flexibility as linker bending and a symmetry decrease were observed in this framework as compared to its structural isomer NPF-300 (Hf). The mesoporous feature and permanent porosity were determined by the N_2 adsorption at 77 K. Such a hierarchical pore feature is expected to enable a variety of applications through encapsulation of large functional molecules. The synthetic strategy of utilizing a mixed solvent and flexible linker is expected to inspire the development of new hafnium MOFs with diverse topological structures.

Keywords: metal–organic frameworks; hafnium; mixed solvent; csq topology; mesoporous MOF

check for updates

Citation: Ma, Y.; Zhang, X. Structure Tuning of Hafnium Metal–Organic Frameworks through a Mixed Solvent Approach. *Crystals* **2022**, *12*, 785. https://doi.org/10.3390/cryst12060785

Academic Editor: Paul R. Raithby

Received: 8 May 2022
Accepted: 25 May 2022
Published: 29 May 2022

1. Introduction

Metal–organic frameworks have attracted considerable attention in the past two decades. [1,2] Their highly tunable pore size [3], ultrahigh surface area [4], and facile functionalization of the pore surface [5,6] enable a variety of applications including in catalysis [7,8], gas storage [9,10], separation [11–14], and luminescence sensing [15,16]. In particular, the recent development of water-stable MOFs has further pushed this emerging type of porous material to more fields involving water, such as proton conduction [17], water purification [18,19], and water harvesting [20] from air. Among water-stable MOFs, zirconium and hafnium with +4 charge exhibit excellent stability [21,22] and also highly tunable topology structures [23–28], which greatly benefit performance optimization through delicate pore tuning.

The highly viable structure of Zr/Hf-MOFs can be attributed to the viable connections of the clusters. For the classical $Zr_6O_4(OH)_4(COO^-)_{12}$ cluster, the maximum connection is twelve. Meanwhile, in MOF formation, the connection can be reduced to eight, six, and four, depending on the symmetry matching as well as the synthetic conditions. For example, diverse Zr-MOFs have been discovered with a tetracarboxyphenylporphyrin (TCPP) linker. In 2012, Yaghi et al. reported two structures: MOF-525 [29] with a twelve-connected cluster, and mesoporous MOF-545/PCN-222 [29,30] with an eight-connected cluster. The topology was **ftw** for MOF-525 and **csq** for MOF-545/PCN-222.

To purposely synthesize new Zr-MOF structures, several strategies have been developed. Through kinetically controlled synthesis, Zr-TCPP MOF (PCN-223) with the **shp-a** topology and a twelve-connected cluster was obtained. [31] In another case, Zr-TCPP MOF (PCN-224) was formed with a six-connected Zr cluster through a linker elimination strategy. [32] Interestingly, even with the same connection, different topologies can be formed. For example, a tetracarboxylate linker and an eight-connected Zr cluster can form

the **scu**, **csq**, and **flu** topologies, and a systematic study revealed that such a topology difference is dependent upon the linker conformation. [33] Such a structure difference could lead to a significant change in application performance, such as for catalysis [34] and gas separation [35]. Therefore, it is of high significance to develop new structures and novel strategies for phase control.

Hafnium MOFs usually form isostructures with Zr-MOFs and exhibit different chemical properties and superior application performance in some cases [36–38]. However, the structural or topology tuning of Hf-MOFs has rarely been reported. In addition, although the structure tuning of Zr-MOFs has been explored, the linker flexibility has not been a consideration thus far. Herein, we report a mesoporous Hf-MOF, namely, csq-MOF-1, using a flexible tetracarboxylate linker, as a structural isomer of NPF-300 (Hf) [39]. The successful synthesis of csq-MOF-1 relies on a mixed solvent approach through a finely tuned DMF/DEF (DMF: dimethyl formamide; DEF: diethyl formamide) mixture ratio. The linker conformation of csq-MOF-1 is in a bending geometry, being different to that of NPF-300 (Hf). The rigid framework csq-MOF-1 also exhibits permanent porosity as revealed by N_2 uptake. This simple mixed solvent approach represents a new strategy to control Hf-MOF topology structures.

2. Materials and Methods

All solvents and reagents were purchased from commercial sources and, unless otherwise noted, used without further purification. The tetracarboxylic ligand linker 5′,5′′′′-(Buta-1,3-diyne-1,4-diyl)bis(([1,1′:3′,1′′-terphenyl]-4,4′′-dicarboxylic acid)) was synthesized according to our previous method in the NPF-300 synthesis [39]. PXRD data were recorded with a PANalytical Empyrean diffractometer (Almelo, The Netherlands) with a PIXcel 3D detector. The copper target X-ray tube was set to 45 kV and 40 mA. Gas adsorption isotherms were collected using the surface area analyzer Micromeritics ASAP-2020 (Norcross, GA, USA). N_2 gas adsorption isotherms were measured at 77 K using a liquid N_2 bath.

The crystal sample was taken from the mother liquid, transferred to oil, and mounted by a loop. Single-crystal X-ray diffraction data were collected using synchrotron radiation. Indexing was performed using APEX2 (difference vector method). Data integration and reduction were performed using SaintPlus 6.0 (Bruker, WI, USA). Absorption correction was performed using a multi-scan method implemented in SADABS. Space groups were determined using XPREP implemented in APEX2. The structure was solved using SHELXS-2014 (direct methods) and refined using SHELXL-2014 within Olex 2 (full-matrix least squares on F^2). Hf, C, and O atoms were refined with anisotropic displacement parameters, and H atoms were placed in geometrically calculated positions and included in the refinement process using a riding model with isotropic thermal parameters: Uiso(H) = 1.2Ueq(-CH). The contribution of disordered solvent molecules was treated as diffuse using the SQUEEZE procedure implemented in PLATON. [40] Crystal structure images were produced using Diamond software by our collaborator at Sun Yat-Sen University.

To activate MOFs for N_2 gas adsorption measurement, as-synthesized MOF samples were exchanged with fresh DMF three times and heated in oven at 80 °C for 4 h. Then, the samples were exchanged with fresh DMF 3 times and subsequently exchanged with anhydrous acetone 6 times in 3 d to remove the DMF completely. The acetone-exchanged samples were decanted and dried in a vacuum oven for 6 h. The dry samples were further de-gassed with the surface area analyzer ASAP 2020 at 80 °C to remove trace amounts of acetone trapped in the pore.

NPF-300-Hf synthesis: Here, 16 mg of $HfCl_4$ and 200 mg of benzoic acid were mixed in a mixed solvent (DMF/DEF = 0.8 mL:0.1 mL) in a glass vial and ultrasonically dissolved. The clear solution was heated in an oven at 80 °C for 1 h. After cooling down to room temperature, 4 mg of ligand was added to this solution, and the mixture was sonicated for 5 min to dissolve all of the ligand. The yellow solution was heated in an oven at 120 °C for 48 h. After cooling down to room temperature, light-yellow, block-shaped single crystals

were obtained. As-synthesized NPF-300-Hf was activated by soaking in fresh DMF at 80 °C for 4 h to remove the unreacted ligand and cluster.

csq-MOF-1 synthesis (single crystal): Here, 16 mg of $HfCl_4$ and 200 mg of benzoic acid were mixed in a mixed solvent (DMF/DEF = 0.1 mL:0.8 mL) in a glass vial and ultrasonically dissolved. The clear solution was heated in an oven at 80 °C for 1 h. After cooling down to room temperature, 4 mg of ligand was added to this solution, and the mixture was sonicated for 5 min to dissolve all of the ligand. The yellow solution was heated in an oven at 120 °C for 48 h. After cooling down to room temperature, light-yellow, block-shaped single crystals were obtained. As-synthesized NPF-300-Hf was activated by soaking in fresh DMF at 80 °C for 4 h to remove the unreacted ligand and cluster.

For the surface area measurement, the csq-MOF-1 sample was synthesized with 15 mg of $HfCl_4$, 5 mg of ligand, 100 mg of benzoic acid, and 0.1 mL of formic acid in a mixed solvent (DMF/DEF = 0.2 mL:0.8 mL), as an optimized synthetic method with a higher yield.

3. Results and Discussion

As it is known that diverse structures of Zr/Hf MOFs can be formed with the same linker, we explored the Hf-MOF structural diversity using a tetracarboxylate linker of NPF-300 due to its flexibility. As discovered in our previous work of linker insertion in NPF-300, the tetracarboxylate linker with a dialkynyl unit could form in-plane and out-of-plane bending to accommodate secondary linkers of different lengths. We were interested in exploring if such flexibility of the linker could affect the formation of diverse topological structures. After extensive attempts under synthetic conditions, we discovered a new structure using solvothermal conditions with a mixed solvent of DMF/DEF at 120 °C for 48 h. The effect of the solvent may be attributed to the different solubilities of precursors or nucleates which alter the crystallization kinetics. The formation of csq-MOF-1 needs a higher amount of DEF with a DMF/DEF ratio of 1:8, in comparison with the DMF/DEF ratio of 8:1 for NPF-300 synthesis. Benzoic acid was used for both cases as a modulator.

The csq-MOF-1 framework crystallizes in a hexagonal crystal system with the *P 6/mmm* space group, as shown in Table 1. Each Hf_6 cluster is coordinated with eight carboxylates from different linkers and eight terminal H_2O/OH^- groups in the equatorial plane. The overall formula of csq-MOF-1 is $Hf_6O_4(OH)_8(H_2O)_4L_2$. The structure has a csq topology, being the same as PCN-222 [30] and NU-1000 [25]. In comparison with NPF-300 with a single type of channel, csq-MOF-1 exhibits two types of channels with triangular and hexagonal geometries, as shown in Figure 1. Such a structural feature is quite interesting due to the intrinsic hierarchical pore structure. The phase purity of csq-MOF-1 was confirmed using PXRD, which showed excellent matching with the patterns simulated from the single-crystal data (Figure 2).

Table 1. Crystal data and structure refinement for csq-MOF-1.

Identification Code	csq-MOF-1
CCDC	2167258
Empirical formula	$C_{44}H_{22}Hf_3O_{16}$
Formula weight	1342.08
Temperature/K	271 (2)
Crystal system	hexagonal
Space group	*P 6/mmm*
a/Å	40.2473 (12)
b/Å	40.2473 (12)
c/Å	20.4333 (11)
α/°	90
β/°	90
γ/°	120

Table 1. *Cont.*

Identification Code	csq-MOF-1
Volume/Å^3	28,664 (2)
Z	6
ρ_{calc}/g cm^{-3}	0.466
μ/mm^{-1}	0.395
F(000)	3780
Crystal size/mm^3	0.5 × 0.1 × 0.1
Radiation	Synchrotron (λ = 0.41325)
2θ range for data collection/°	0.672 to 14.069
Index ranges	$-47 \leq h \leq 47$, $-47 \leq k \leq 47$, $-24 \leq l \leq 24$
Reflections collected	588,792
Independent reflections	9026 [R(int) = 0.1355]
Data/restraints/parameters	9026/0/159
Goodness of fit on F^2	1.496
Final R indexes [$I \geq 2\sigma$ (I)]	R_1 = 0.0810 wR_2 = 0.2449
Final R indexes (all data)	R_1 = 0.0985, wR_2 = 0.2589
Largest diff. peak/hole/e Å^{-3}	1.345 and −1.915

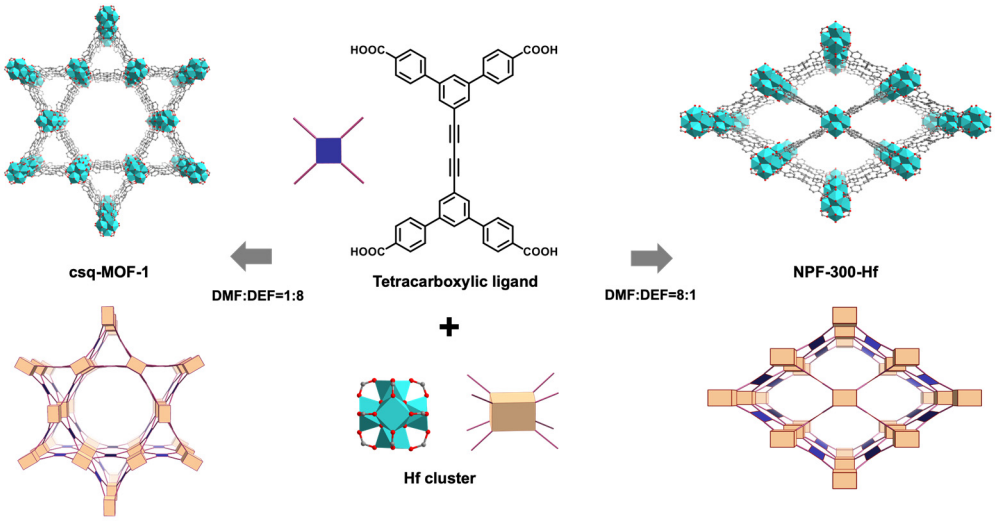

Figure 1. Synthesis, structure, and topological representation of csq-MOF-1 in comparison with NPF-300 (Hf).

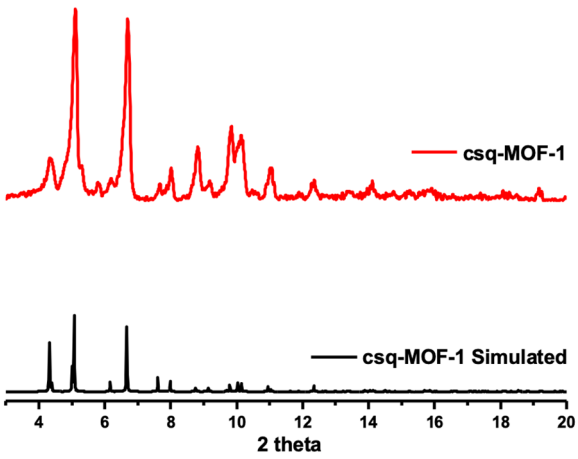

Figure 2. PXRD of csq-MOF-1 in comparison with simulated patterns from a single-crystal structure.

A close examination of csq-MOF-1 revealed that the ligand flexibility is quite important in the structure formation. As shown in Figure 3a, the structure view along the b axis clearly shows out-of-plane bending of the tetracarboxylate linker. In NPF-300, the linker is planar with a C2h symmetry, while the out-of-plane bending of the linker causes its symmetry to decrease to the Cs point group in the csq-MOF-1 structure. The linker bending also leads to a decrease in the cluster distance along the c axis from 13.198 Å of NPF-300 to 12.618 Å of csq-MOF-1. Such a difference in the cluster distance is potentially more favorable for the insertion of a shorter linker. The hexagonal channel exhibits the largest dimension of ~32.238 Å, being much larger than that of NPF-300 (12.660 Å), as shown in Figure 3c,d.

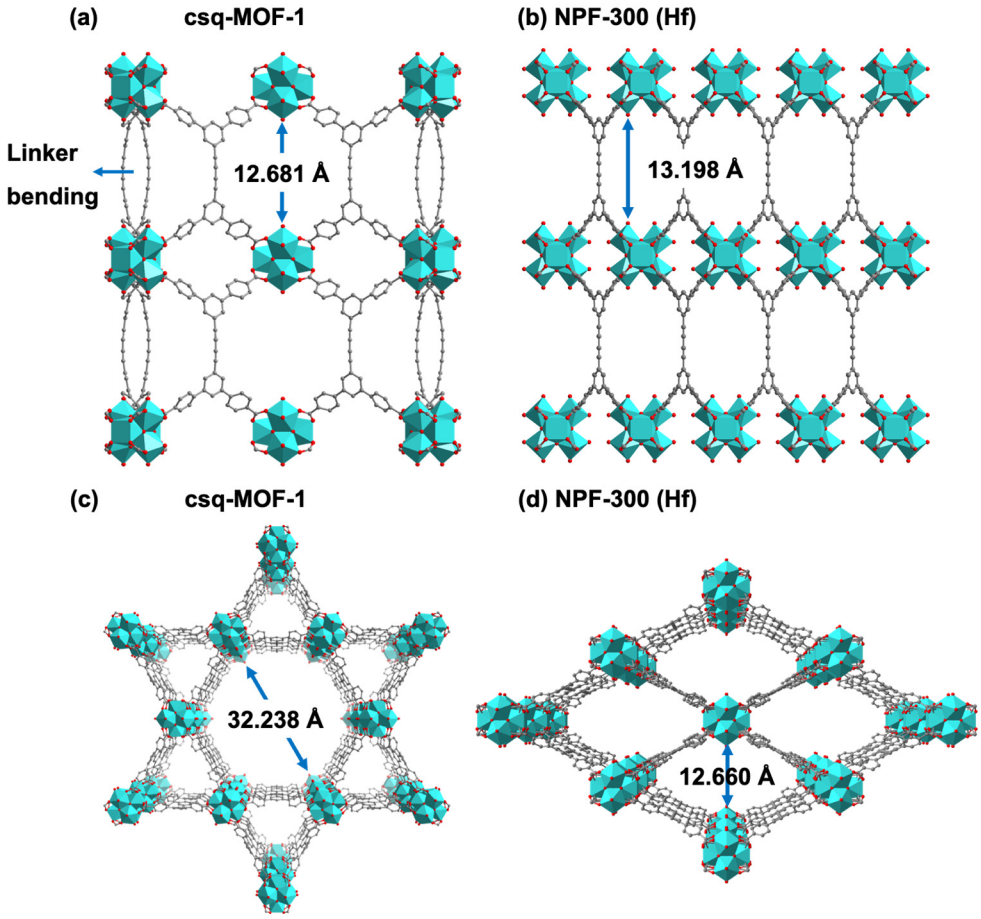

Figure 3. Structures viewed along the b axis and c axis. (**a**) Structure of csq-MOF-1, showing linker bending, cluster distance; (**b**) structure of NPF-300 (Hf), showing planar linker, cluster distance. (**c**) channel of csq-MOF-1; (**d**) channel of NPF-300 (Hf). Hf: cyan polyhedron; C: light gray; O: red; hydrogen atoms are omitted for clarity.

The mesoporous feature was further validated by the N_2 adsorption isotherm at 77 K. As shown in Figure 4a, a sudden increase in uptake was observed, which can be attributed to the capillary condensation of the N_2 gas in the mesopore. Based on the adsorption isotherm, the surface area of csq-1 was determined as 1735 m^2/g using the BET (Brunauer–Emmett–Teller) method and 1986 m^2/g using the Langmuir method. Further, the total pore volume was determined as 1.1 cm^3/g, and all these results demonstrate the high permanent porosity of csq-MOF-1. The pore size distribution showed two major pore sizes: micropores of ~15 Å, and mesopores of ~30 Å, being consistent with the hierarchical pore feature determined from the single-crystal structure. Such a mesoporous Hf-MOF is expected to be useful for the encapsulation of large guest molecules such as enzymes, protein drugs, and metal nanoparticles for a broad scope of applications.

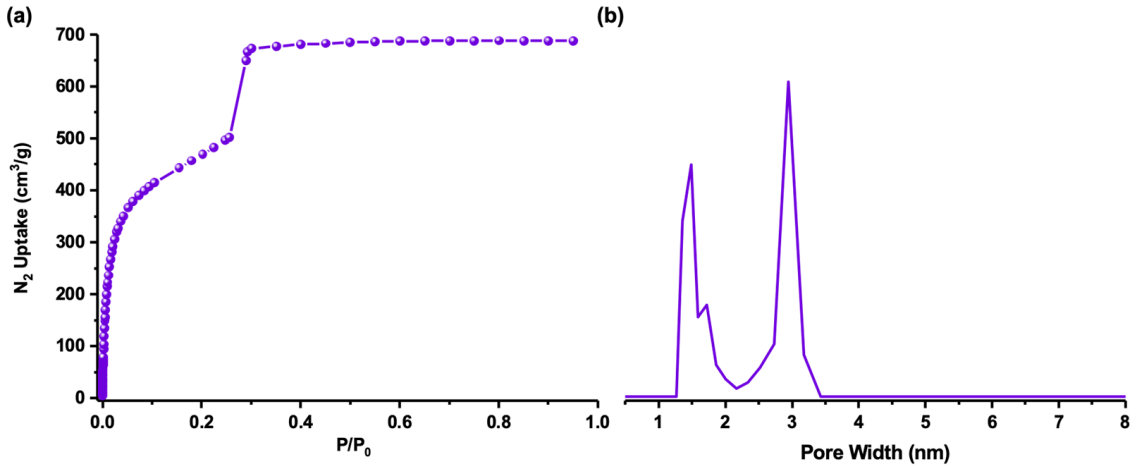

Figure 4. N_2 adsorption isotherm at 77 K (**a**) and pore size distribution of csq-MOF-1 (**b**).

4. Results and Discussion

In summary, we report a new mesoporous Hf-MOF using a mixed solvent approach to control the topology. The resulting csq-MOF-1 exhibits a csq topology and large hexagonal channels of ~ 32 Å. The ligand linker in csq-MOF-1 is in a bending geometry with a decreased symmetry, as compared with the isostructural MOF NPF-300-Hf. The permanent porosity and mesoporous feature were demonstrated by a N_2 adsorption experiment, and a high BET surface area of 1735 m^2/g was calculated based on the adsorption isotherm. The new MOF structural feature and structure tuning strategy are expected to inspire the development of diverse Hf-MOF structures and further broaden their application scope.

Author Contributions: Conceptualization, Y.M. and X.Z.; methodology, Y.M. and X.Z.; software, Y.M. and X.Z.; validation, Y.M. and X.Z.; formal analysis, X.Z.; investigation, Y.M. and X.Z.; resources, Y.M. and X.Z.; data curation, Y.M.; writing—original draft preparation, Y.M. and X.Z.; writing—review and editing, X.Z.; visualization, Y.M. and X.Z.; supervision, X.Z.; project administration, X.Z.; funding acquisition, Y.M. All authors have read and agreed to the published version of the manuscript.

Funding: This research was funded by the Guangdong Province General Colleges and Universities Youth Innovative Talents Project (Grant No. 2018GkQNCX019).

Institutional Review Board Statement: Not applicable.

Informed Consent Statement: Not applicable.

Data Availability Statement: Crystal structure data can be found at the Cambridge Crystallographic Data Centre website (No. 2167258): https://www.ccdc.cam.ac.uk (accessed on 28 May 2022).

Acknowledgments: The authors are grateful for the financial support from the Guangdong Province General Colleges and Universities Youth Innovative Talents Project (Grant No. 2018GkQNCX019).

Conflicts of Interest: The authors declare no conflict of interest.

References

1. Furukawa, H.; Cordova, K.E.; O'Keeffe, M.; Yaghi, O.M. The chemistry and applications of metal-organic frameworks. *Science* **2013**, *341*, 1230444. [CrossRef] [PubMed]
2. Belver, C.; Bedia, J. Metal Organic Frameworks for Advanced Applications. *Catalysts* **2021**, *11*, 648. [CrossRef]
3. Fan, L.; Zhou, P.; Wang, X.; Yue, L.; Li, L.; He, Y. Rational Construction and Performance Regulation of an In(III)-Tetraisophthalate Framework for One-Step Adsorption-Phase Purification of C_2H_4 from C_2 Hydrocarbons. *Inorg. Chem.* **2021**, *60*, 10819–10829. [CrossRef]
4. Zhang, X.; Zhang, X.; Johnson, J.A.; Chen, Y.-S.; Zhang, J. Highly Porous Zirconium Metal-Organic Frameworks with beta-UH3-like Topology Based on Elongated Tetrahedral Linkers. *J. Am. Chem. Soc.* **2016**, *138*, 8380–8383. [CrossRef] [PubMed]
5. Lu, Z.; Li, Y.; Ru, Y.; Yang, S.; Hao, C.; Zuo, M.; Jiao, R.; Yao, H. The Structure and Property of Two Different Metal-Organic Frameworks Based on N/O-Donor Mixed Ligands. *Crystals* **2021**, *11*, 1129. [CrossRef]

6. Manna, B.; Sharma, S.; Ghosh, S. Synthesis and Crystal Structure of a Zn(II)-Based MOF Bearing Neutral N-Donor Linker and SiF62—Anion. *Crystals* **2018**, *8*, 37. [CrossRef]
7. Heu, R.; Ateia, M.; Yoshimura, C. Photocatalytic Nanofiltration Membrane Using Zr-MOF/GO Nanocomposite with High-Flux and Anti-Fouling Properties. *Catalysts* **2020**, *10*, 711. [CrossRef]
8. Ji, P.; Manna, K.; Lin, Z.; Urban, A.; Greene, F.X.; Lan, G.; Lin, W. Single-Site Cobalt Catalysts at New $Zr_8(\mu_2\text{-}O)_8(\mu_2\text{-}OH)_4$ Metal-Organic Framework Nodes for Highly Active Hydrogenation of Alkenes, Imines, Carbonyls, and Heterocycles. *J. Am. Chem. Soc.* **2016**, *138*, 12234–12242. [CrossRef]
9. He, Y.; Zhou, W.; Yildirim, T.; Chen, B. A series of metal–organic frameworks with high methane uptake and an empirical equation for predicting methane storage capacity. *Energy Environ. Sci.* **2013**, *6*, 2735. [CrossRef]
10. Zhang, X.; Lin, R.B.; Wang, J.; Wang, B.; Liang, B.; Yildirim, T.; Zhang, J.; Zhou, W.; Chen, B. Optimization of the Pore Structures of MOFs for Record High Hydrogen Volumetric Working Capacity. *Adv. Mater.* **2020**, *32*, e1907995. [CrossRef]
11. Lin, R.B.; Li, L.; Zhou, H.L.; Wu, H.; He, C.; Li, S.; Krishna, R.; Li, J.; Zhou, W.; Chen, B. Molecular sieving of ethylene from ethane using a rigid metal-organic framework. *Nat. Mater.* **2018**, *17*, 1128–1133. [CrossRef] [PubMed]
12. Zhang, X.; Lin, R.-B.; Wu, H.; Huang, Y.; Ye, Y.; Duan, J.; Zhou, W.; Li, J.-R.; Chen, B. Maximizing acetylene packing density for highly efficient C_2H_2/CO_2 separation through immobilization of amine sites within a prototype MOF. *Chem. Eng. J.* **2022**, *431*, 134184. [CrossRef]
13. Cadiau, A.; Adil, K.; Bhatt, P.M.; Belmabkhout, Y.; Eddaoudi, M. A metal-organic framework-based splitter for separating propylene from propane. *Science* **2016**, *353*, 137–140. [CrossRef] [PubMed]
14. Jiang, Z.; Fan, L.; Zhou, P.; Xu, T.; Hu, S.; Chen, J.; Chen, D.-L.; He, Y. An aromatic-rich cage-based MOF with inorganic chloride ions decorating the pore surface displaying the preferential adsorption of C_2H_2 and C_2H_6 over C_2H_4. *Inorg. Chem. Front.* **2021**, *8*, 1243–1252. [CrossRef]
15. Wang, B.; Lv, X.L.; Feng, D.; Xie, L.H.; Zhang, J.; Li, M.; Xie, Y.; Li, J.R.; Zhou, H.C. Highly Stable Zr(IV)-Based Metal-Organic Frameworks for the Detection and Removal of Antibiotics and Organic Explosives in Water. *J. Am. Chem. Soc.* **2016**, *138*, 6204–6216. [CrossRef]
16. Zhao, Y.-L.; Chen, Q.; Lv, J.; Xu, M.-M.; Zhang, X.; Li, J.-R. Specific sensing of antibiotics with metal-organic frameworks based dual sensor system. *Nano Res.* **2022**. [CrossRef]
17. Ye, Y.; Gong, L.; Xiang, S.; Zhang, Z.; Chen, B. Metal-Organic Frameworks as a Versatile Platform for Proton Conductors. *Adv. Mater.* **2020**, *32*, 1907090. [CrossRef]
18. Pournara, A.D.; Andreou, E.K.; Armatas, G.S.; Manos, M.J. Zirconium(IV) Metal Organic Frameworks with Highly Selective Sorption for Diclofenac under Batch and Continuous Flow Conditions. *Crystals* **2022**, *12*, 424. [CrossRef]
19. Gao, Y.; Pan, Y.; Zhou, Z.; Tian, Q.; Jiang, R. The Carboxyl Functionalized UiO-66-$(COOH)_2$ for Selective Adsorption of Sr^{2+}. *Molecules* **2022**, *27*, 1208. [CrossRef]
20. Kalmutzki, M.J.; Diercks, C.S.; Yaghi, O.M. Metal-Organic Frameworks for Water Harvesting from Air. *Adv. Mater.* **2018**, *30*, e1704304. [CrossRef]
21. Bai, Y.; Dou, Y.; Xie, L.H.; Rutledge, W.; Li, J.R.; Zhou, H.C. Zr-based metal-organic frameworks: Design, synthesis, structure, and applications. *Chem. Soc. Rev.* **2016**, *45*, 2327–2367. [CrossRef] [PubMed]
22. Zhang, X.; Wang, B.; Alsalme, A.; Xiang, S.; Zhang, Z.; Chen, B. Design and applications of water-stable metal-organic frameworks: Status and challenges. *Coord. Chem. Rev.* **2020**, *423*, 213507. [CrossRef]
23. Krause, S.; Bon, V.; Stoeck, U.; Senkovska, I.; Tobbens, D.M.; Wallacher, D.; Kaskel, S. A Stimuli-Responsive Zirconium Metal-Organic Framework Based on Supermolecular Design. *Angew. Chem. Int. Ed.* **2017**, *56*, 10676–10680. [CrossRef] [PubMed]
24. Zhang, M.; Chen, Y.P.; Bosch, M.; Gentle, T., 3rd; Wang, K.; Feng, D.; Wang, Z.U.; Zhou, H.C. Symmetry-guided synthesis of highly porous metal-organic frameworks with fluorite topology. *Angew. Chem. Int. Ed.* **2014**, *53*, 815–818. [CrossRef] [PubMed]
25. Mondloch, J.E.; Bury, W.; Fairen-Jimenez, D.; Kwon, S.; DeMarco, E.J.; Weston, M.H.; Sarjeant, A.A.; Nguyen, S.T.; Stair, P.C.; Snurr, R.Q.; et al. Vapor-phase metalation by atomic layer deposition in a metal-organic framework. *J. Am. Chem. Soc.* **2013**, *135*, 10294–10297. [CrossRef]
26. Wang, T.C.; Bury, W.; Gomez-Gualdron, D.A.; Vermeulen, N.A.; Mondloch, J.E.; Deria, P.; Zhang, K.; Moghadam, P.Z.; Sarjeant, A.A.; Snurr, R.Q.; et al. Ultrahigh surface area zirconium MOFs and insights into the applicability of the BET theory. *J. Am. Chem. Soc.* **2015**, *137*, 3585–3591. [CrossRef]
27. Zhang, Y.; Zhang, X.; Lyu, J.; Otake, K.I.; Wang, X.; Redfern, L.R.; Malliakas, C.D.; Li, Z.; Islamoglu, T.; Wang, B.; et al. A Flexible Metal-Organic Framework with 4-Connected Zr_6 Nodes. *J. Am. Chem. Soc.* **2018**, *140*, 11179–11183. [CrossRef]
28. Lin, Q.; Bu, X.; Kong, A.; Mao, C.; Zhao, X.; Bu, F.; Feng, P. New heterometallic zirconium metalloporphyrin frameworks and their heteroatom-activated high-surface-area carbon derivatives. *J. Am. Chem. Soc.* **2015**, *137*, 2235–2238. [CrossRef]
29. Morris, W.; Volosskiy, B.; Demir, S.; Gandara, F.; McGrier, P.L.; Furukawa, H.; Cascio, D.; Stoddart, J.F.; Yaghi, O.M. Synthesis, structure, and metalation of two new highly porous zirconium metal-organic frameworks. *Inorg. Chem.* **2012**, *51*, 6443–6445. [CrossRef]
30. Feng, D.; Gu, Z.Y.; Li, J.R.; Jiang, H.L.; Wei, Z.; Zhou, H.C. Zirconium-metalloporphyrin PCN-222: Mesoporous metal-organic frameworks with ultrahigh stability as biomimetic catalysts. *Angew. Chem. Int. Ed.* **2012**, *51*, 10307–10310. [CrossRef]
31. Feng, D.; Gu, Z.Y.; Chen, Y.P.; Park, J.; Wei, Z.; Sun, Y.; Bosch, M.; Yuan, S.; Zhou, H.C. A highly stable porphyrinic zirconium metal-organic framework with shp-a topology. *J. Am. Chem. Soc.* **2014**, *136*, 17714–17717. [CrossRef] [PubMed]

32. Feng, D.; Chung, W.C.; Wei, Z.; Gu, Z.Y.; Jiang, H.L.; Chen, Y.P.; Darensbourg, D.J.; Zhou, H.C. Construction of ultrastable porphyrin Zr metal-organic frameworks through linker elimination. *J. Am. Chem. Soc.* **2013**, *135*, 17105–17110. [CrossRef] [PubMed]
33. Pang, J.; Yuan, S.; Qin, J.; Liu, C.; Lollar, C.; Wu, M.; Yuan, D.; Zhou, H.C.; Hong, M. Control the Structure of Zr-Tetracarboxylate Frameworks through Steric Tuning. *J. Am. Chem. Soc.* **2017**, *139*, 16939–16945. [CrossRef] [PubMed]
34. Lyu, J.; Zhang, X.; Otake, K.I.; Wang, X.; Li, P.; Li, Z.; Chen, Z.; Zhang, Y.; Wasson, M.C.; Yang, Y.; et al. Topology and porosity control of metal-organic frameworks through linker functionalization. *Chem. Sci.* **2019**, *10*, 1186–1192. [CrossRef] [PubMed]
35. Wang, H.; Dong, X.; Lin, J.; Teat, S.J.; Jensen, S.; Cure, J.; Alexandrov, E.V.; Xia, Q.; Tan, K.; Wang, Q.; et al. Topologically guided tuning of Zr-MOF pore structures for highly selective separation of C6 alkane isomers. *Nat. Commun.* **2018**, *9*, 1745. [CrossRef] [PubMed]
36. Beyzavi, M.H.; Klet, R.C.; Tussupbayev, S.; Borycz, J.; Vermeulen, N.A.; Cramer, C.J.; Stoddart, J.F.; Hupp, J.T.; Farha, O.K. A hafnium-based metal-organic framework as an efficient and multifunctional catalyst for facile CO2 fixation and regioselective and enantioretentive epoxide activation. *J. Am. Chem. Soc.* **2014**, *136*, 15861–15864. [CrossRef]
37. Beyzavi, M.H.; Vermeulen, N.A.; Howarth, A.J.; Tussupbayev, S.; League, A.B.; Schweitzer, N.M.; Gallagher, J.R.; Platero-Prats, A.E.; Hafezi, N.; Sarjeant, A.A.; et al. A Hafnium-Based Metal-Organic Framework as a Nature-Inspired Tandem Reaction Catalyst. *J. Am. Chem. Soc.* **2015**, *137*, 13624–13631. [CrossRef]
38. Wang, C.; Volotskova, O.; Lu, K.; Ahmad, M.; Sun, C.; Xing, L.; Lin, W. Synergistic assembly of heavy metal clusters and luminescent organic bridging ligands in metal-organic frameworks for highly efficient X-ray scintillation. *J. Am. Chem. Soc.* **2014**, *136*, 6171–6174. [CrossRef]
39. Zhang, X.; Frey, B.L.; Chen, Y.-S.; Zhang, J. Topology-Guided Stepwise Insertion of Three Secondary Linkers in Zirconium Metal-Organic Frameworks. *J. Am. Chem. Soc.* **2018**, *140*, 7710–7715. [CrossRef]
40. Spek, A.L. Single-crystal structure validation with the program PLATON. *J. Appl. Crystallogr.* **2003**, *36*, 7–13. [CrossRef]